Electronic Supplementary Material (ESI) for Chemical Science.
This journal is © The Royal Society of Chemistry 2020

Electronic Supplementary Information for:

Hierarchical Nanosheets Built from Superatomic Clusters: Properties, Exfoliation and Single-Crystal-to-Single-Crystal Intercalation

Jonathan A. Kephart[1], Catherine G. Romero[1], Chun-Chih Tseng[2], Kevin J. Anderton[3], Matthew Yankowitz[2,4], Werner Kaminsky[1], Alexandra Velian[1]*

[1]Department of Chemistry, University of Washington, Seattle, Washington 98195, United States; [2]Department of Physics, University of Washington, Seattle, Washington 98195, United States; [3]Department of Chemistry and Chemical Biology, Harvard University, Cambridge, Massachusetts 02138, United States; [4]Department of Materials Science and Engineering, University of Washington, Seattle, Washington 98195, United States

Table of Contents

S1 General Considerations

All syntheses were conducted under a dinitrogen atmosphere using a standard Schlenk line or an LC Technology Solutions glovebox equipped with a freezer set to −35 °C. All glassware was dried at 160 °C for a minimum of 12 h prior to use.

Solvents were purchased from Fischer Scientific and degassed, dried and purified using solvent purification columns housed in a stainless-steel cabinet and dispensed by a stainless-steel Schlenk line manufactured by JC Meyer Solvent Systems. Tetrahydrofuran (THF), diethyl ether (Et_2O), acetonitrile (MeCN), and methylene chloride (DCM) are passed through two packed columns of neutral alumina. *n*-Pentane and toluene are passed through a column packed with alumina, and one containing Q5 reactant, a copper(II) oxide oxygen scavenger. All solvents were passed through an in-line, 2 µm filter, then stored over activated 3Å molecular sieves in the glovebox. 3Å molecular sieves were purchased from Sigma Aldrich and activated under vacuum at 300 °C for 48 h. Anhydrous pyridine (99.8%) was purchased from Sigma Aldrich and stored over activated 3Å molecular sieves for 72 h prior to use.

Deuterated solvents ($CDCl_3$, C_6D_6, CD_2Cl_2, CD_3CN) were purchased from Cambridge Isotope Laboratories, Inc., degassed and dried over activated 3Å molecular sieves in the glovebox for a minimum of 72 h. $CoCl_2$ (98+%) was purchased from Strem Chemicals, Inc. and dried under vacuum at 120 °C for 24 h prior to use. $Co_2(CO)_8$ (stabilized with 2-5% hexanes; Strem Chemicals, Inc.) was stored in the glovebox freezer and used as received. The aminophosphine $Ph_2PNHTol$ (Ph = phenyl, Tol = 4-tolyl),[1] $Co_6Se_8L^H{}_6$ and $Li_6(py)_6Co_6Se_8L_6$ were prepared according to the literature.[2] Chlorodiphenylphosphine (97%) and *p*-toluidine (99+%) were purchased from Alfa Aesar and used without further purification. Selenium (99.5%, powder, 200 mesh), *n*-butyl lithium (2.5 M in hexanes), 4,4'-bipyridine (98%), 1,2-bis(4-pyridyl)ethane (99%), and 1,2-di(4-pyridyl)ethylene (97%) were purchased from Sigma Aldrich and used without further purification. Tetracyanoethylene (TCNE, 98%) was purchased from Sigma Aldrich, purified by sublimation, and stored in the dark at –35 °C prior to use.

Atomic force microscopy (AFM) images were acquired on a Bruker Dimension Icon housed within an MBraun LABstar argon glovebox. AFM samples were prepared via mechanical exfoliation of bulk crystalline material. The exfoliated flakes were deposited and analyzed on plasma-cleaned 285 nm SiO_2/Si wafers. Thin flakes of **2-bpy$_\sigma$** were first identified by optical microscopy, and then their thickness was determined by AFM. Throughout the exfoliation process, flakes were prepared, handled, and imaged in an argon atmosphere.

Direct current (dc) magnetic susceptibility data for **1** and **2-bpy$_\pi$** were collected on warming from 2 to 300 K with applied fields of 0.1, 0.5 and 1 T using a Quantum Design MPMS3 Evercool SQUID Magnetometer. These samples were prepared by loading a gelatin capsule (size #4) with polycrystalline material, followed by molten eicosane. dc Magnetic susceptibility data for **2-bpy** and **2-bpy$_\sigma$** were collected on warming from 5 to 300 K under applied fields of 0.1, 0.5, and 1 T using a Quantum Design PPMS DynaCool equipped with a 14 T magnet. To prepare these samples, polycrystalline material was loaded within a gelatin capsule sealed with Kapton tape. In each case, crushed crystalline material placed under vacuum at 90 °C prior to analysis. All magnetic susceptibility data was corrected for diamagnetic contributions from the analyte calculated using Pascal's constants,[3] as well as for the susceptibility of the capsule, sample holder and eicosane. Magnetization data was recorded at 100 K between 0 and 7 T to confirm the absence of any ferromagnetic impurities. Magnetic susceptibility data recorded under different applied fields does not decrease with increasing field strength, indicating that the samples are free of any ferromagnetic impurities. Reduced magnetization data were collected for **1** between 1.8 and 10 K under applied fields between 1.0 and 7.0 T. Susceptibility data for **1** were modeled using PHI in order to extract the g-value, but a quantitative model was not developed due to the complexity of the system.[4]

Cyclic voltammetry was conducted using a µAutolabIII/FRA2 potentiostat by Metrohm. A three-electrode cell setup was used with a glassy carbon disk working electrode, a platinum wire counter electrode, and a

silver-wire pseudo-reference electrode. All potentials were referenced to the Fc/Fc^+ redox couple by adding a small amount of ferrocene after each measurement. All electrochemical measurements were conducted under a dinitrogen atmosphere, at room temperature (ca. 25 °C).

Samples were prepared for elemental analysis by crushing single crystalline material into a powder and then placed under reduced pressure for 12 h. Co, Se, P elemental analysis was conducted using a Perkin-Elmer Nexion 2000B inductively-coupled plasma mass spectrometer (ICP-MS). Prior to ICP-MS analysis, samples were digested in neat nitric acid (Fisher Scientific, ICP-MS grade) at 50 °C.

Scanning electron microscopy (SEM) imaging was performed using a Sirion FEI XL30 at 5 kV for crystalline material dropcast on a 285 nm SiO_2/Si wafer.

UV-vis-*n*IR absorption spectra were acquired using a Varian Cary 5000 UV-Vis-*n*IR spectrophotometer, in *n*IR quartz cuvettes (Spectrocell Inc., 10 mm path length, 220–3500 nm spectral window).

NMR spectra were acquired at 25 °C on Bruker AV300 or AV500 spectrometers. ^{1}H NMR spectra were referenced to residual deuterated solvent peaks.

S2 Synthetic Details and Characterization of Products

S2.1 Synthesis and Isolation of $Co_3(py)_3Co_6Se_8L_6$ (1)

A 350 mL Schlenk tube equipped with a Teflon valve and a magnetic stir bar was loaded with $Li_6(py)_6Co_6Se_8L_6$ (4.000 g, 1.232 mmol, 1 equiv), toluene (144 mL), and THF (6 mL). The sample was partially frozen using the glovebox cold well. Solid $CoCl_2$ (0.480 g, 3.70 mmol, 3.0 equiv) was added portion wise to the thawing, stirring slurry. The flask was sealed, slowly warmed to 25 °C, and then heated at 60 °C for 14 h. Over the course of this time, the initially red-brown slurry homogenized to yield a deep-red solution. Volatiles were removed under reduced pressure, and the crude material was triturated with diethyl ether (3 x 20 mL) to remove excess THF and pyridine. The resulting solids were dissolved in DCM (40 mL), and the mixture passed through a plug of Celite on a fritted glass funnel. Volatiles were removed from the DCM filtrate under reduced pressure. The solids were triturated once more with diethyl ether (15 mL), and then stirred in acetonitrile (30 mL). The solids of this suspension were collected on a fine-porosity fritted glass funnel. These solids were washed with additional acetonitrile (2 x 20 mL) and diethyl ether (10 mL) before being dissolved in THF (50 mL) and filtered. The THF filtrate was layered with diethyl ether (50 mL) and *n*-pentane (100 mL). This layered mixture was kept still at 25 °C for 48 h, yielding a crop of large prismatic crystals. The crystals were collected on a fine porosity fritted glass funnel, and the filtrate was layered with additional *n*-pentane (50 mL) to produce a second crop of crystals. The separate crops of crystals were combined, and volatiles were removed *in vacuo* to yield $Co_3(py)_3Co_6Se_8L_6$ (3.1256 g, 0.995 mmol, 81%) as a dark red, crystalline solid.

^{1}H NMR (C_6D_6, 300 MHz) δ: 75.63 (s, $\nu_{1/2}$ = 1288 Hz); 47.74 (s, $\nu_{1/2}$ = 1935 Hz); 36.60 (s, $\nu_{1/2}$ = 476 Hz), 33.97 (s, 12H, $\nu_{1/2}$ = 722 Hz); 20.98 (s, 12H, $\nu_{1/2}$ = 748 Hz); 14.21 (s, $\nu_{1/2}$ = 1774 Hz); 10.85 (s, $\nu_{1/2}$ = 1402 Hz); –0.13 (s, $\nu_{1/2}$ = 124 Hz); –50.84 (s, $\nu_{1/2}$ = 2993 Hz) ppm. ^{1}H NMR (d_5-pyr, 300 MHz) δ: 34.44 (s, $\nu_{1/2}$ = 83 Hz); 19.95 (s, $\nu_{1/2}$ = 194 Hz); 15.80 (s, $\nu_{1/2}$ = 153 Hz), 13.11 (s, 12H, $\nu_{1/2}$ = 136 Hz); 10.83 (s, $\nu_{1/2}$ = 117 Hz); 4.67 (s, $\nu_{1/2}$ = 211 Hz); –54.10 (s, $\nu_{1/2}$ = 1081 Hz) ppm. μ_{eff} (Evans Method, CD_2Cl_2, 300K): 7.5 μ_B. Elemental analysis found (calc.) for $Co_3(py)_3Co_6Se_8L_6$ (Formula: $C_{129}H_{117}Co_9N_9P_6Se_8$): Co 16.73 (16.88), Se 18.73 (20.11), P 7.30 (5.92).

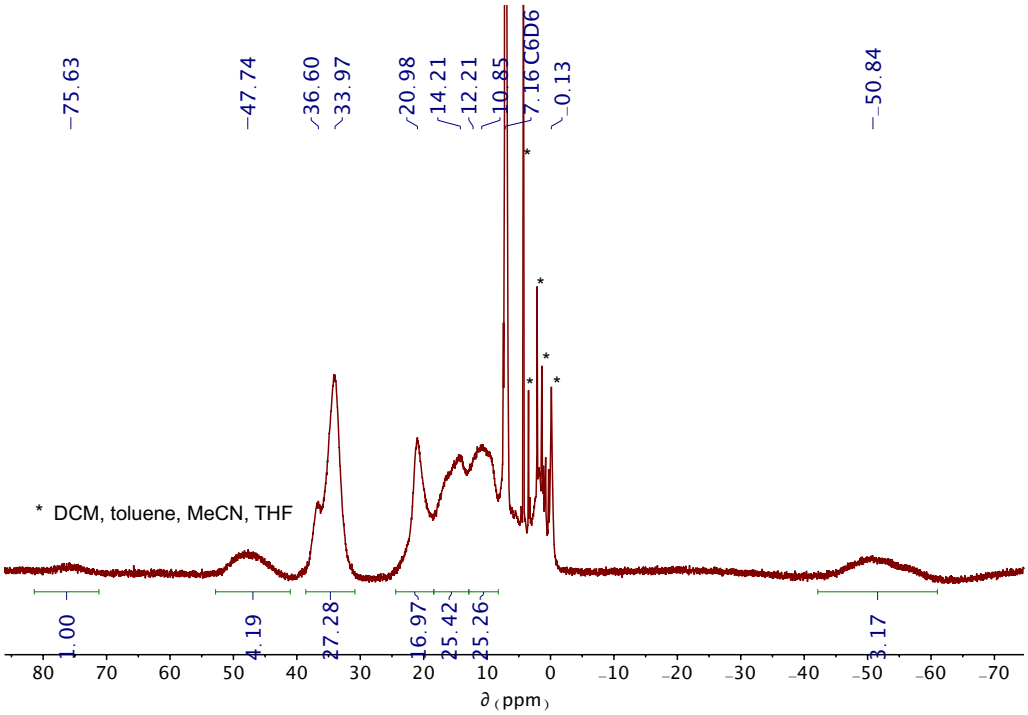

Figure S1. ^{1}H NMR (C_6D_6, 25 °C, 300 MHz) spectrum of $Co_3(py)_3Co_6Se_8L_6$ (**1**).

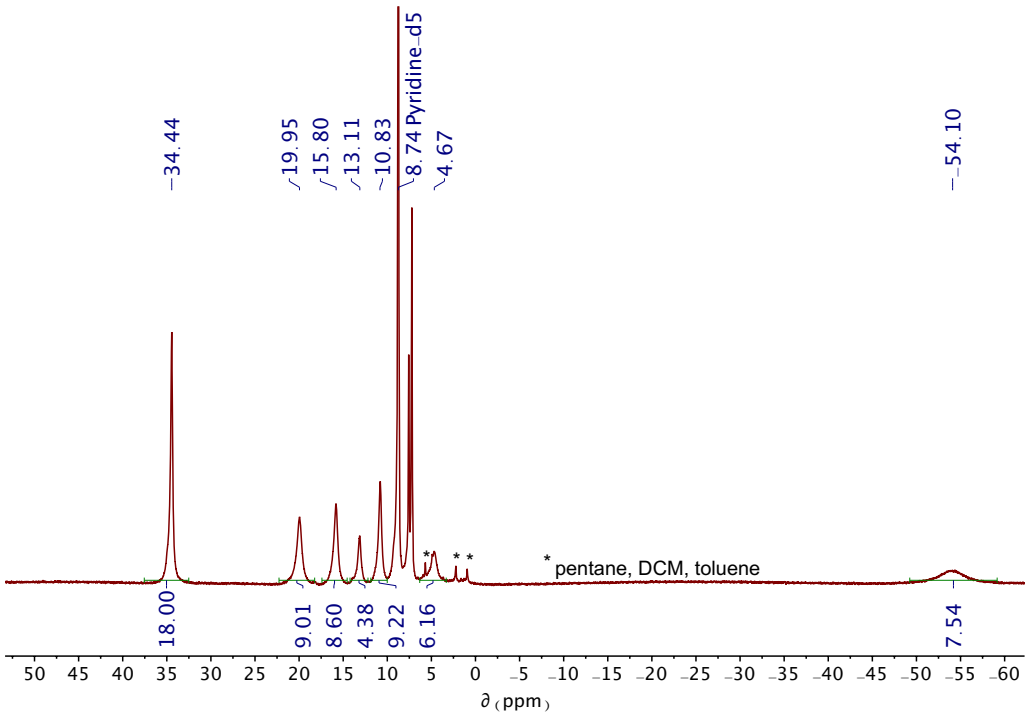

Figure S2. ^{1}H NMR (d_5-pyridine, 25 °C, 300 MHz) spectrum of $Co_3(py)_3Co_6Se_8L_6$ (**1**).

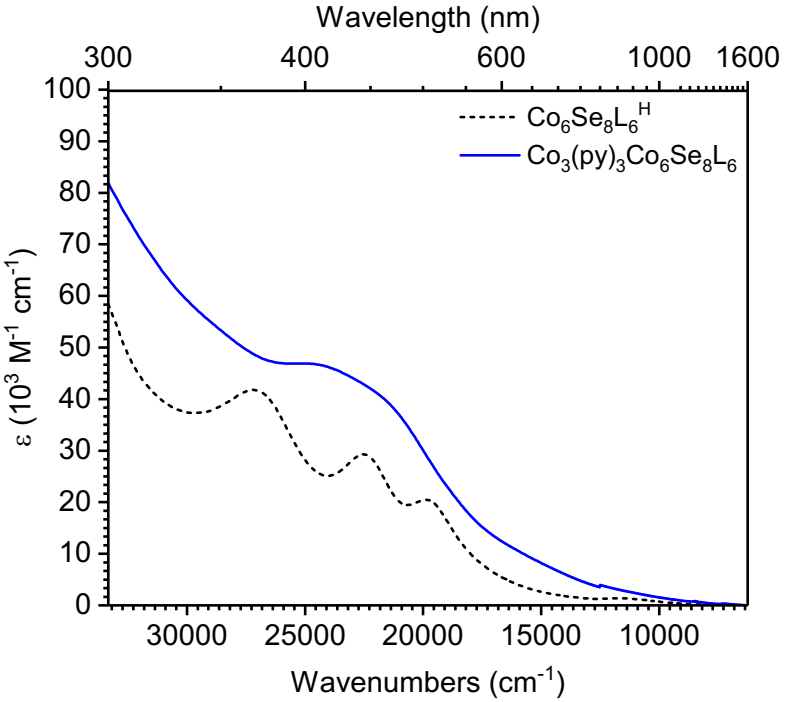

Figure S3. UV-visible absorption spectra of $Co_3(py)_3Co_6Se_8L_6$ (**1**) and $Co_6Se_8L^H{}_6$ recorded in THF.

S2.2 Synthesis and Isolation of $Co_3(bpy)_{1.5}Co_6Se_8L_6$ (2-bpy)

A 20 mL scintillation vial was loaded with $Co_3(py)_3Co_6Se_8L_6$ (100 mg, 0.032 mmol, 1 equiv) and DCM (8 mL). A separate 20 mL scintillation vial was loaded with 4,4'-bipyridine (bpy; 7.5 mg, 0.048 mmol, 1.5 equiv). The solution of $Co_3(py)_3Co_6Se_8L_6$ was passed through a plug of Celite into the vial containing 4,4'-bipyridine. The filter cake was rinsed with DCM (2 mL) and then sample was kept still at 25 °C for 48 h. Dark prismatic crystals formed along the walls of the vial within 12 h. After 48 h, the mother liquor was decanted, and crystals were soaked in DCM (5 x 3 mL; 15 minutes each cycle), decanting the supernatant after each treatment. Volatiles were removed under reduced pressure at 90 °C for 12 h to yield $Co_3(bpy)_{1.5}Co_6Se_8L_6$ (**2-bpy**; 55 mg, 0.018 mmol, 55%) as a dark red crystalline solid. The crystals are insoluble in DCM and toluene, but readily dissolve in d_5-pyridine. ^{1}H NMR analysis reveals in the latter case clean conversion to $Co_3(py)_3Co_6Se_8L_6$ and the bpy linker (Figure S4).

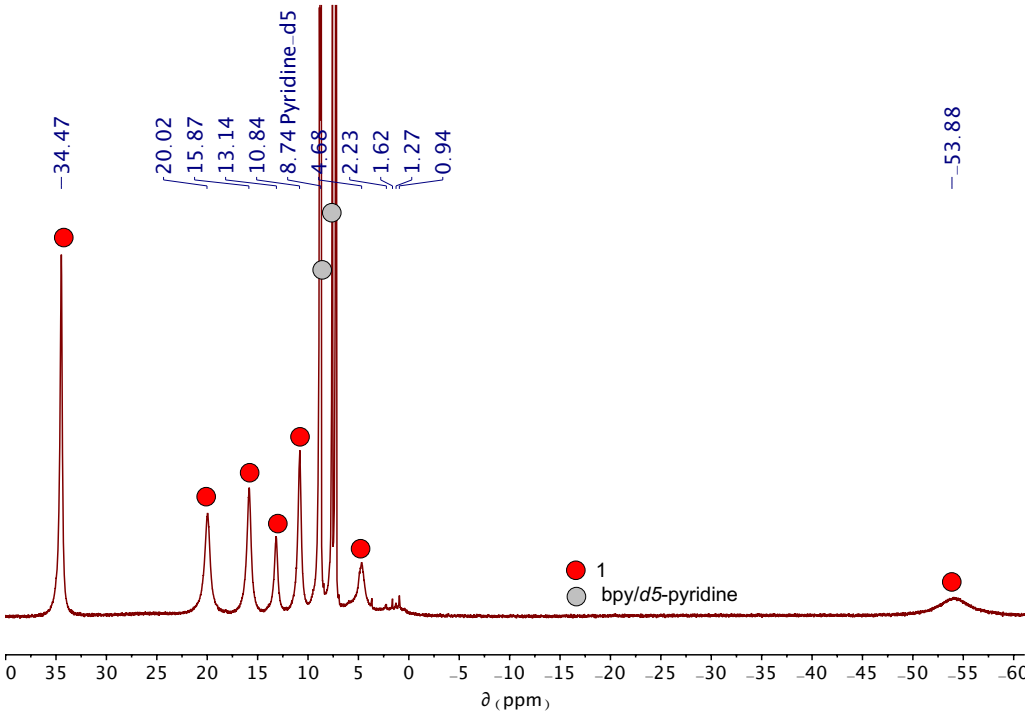

Figure S4. ^{1}H NMR (d_5-pyr, 25 °C, 300 MHz) analysis of **2-bpy** post-dissolution in d_5-pyridine.

S2.3 Synthesis and Isolation of $Co_3(bpy_\pi)_{1.5}Co_6Se_8L_6$ (2-bpy_π)

A 20 mL scintillation vial was loaded with $Co_3(py)_3Co_6Se_8L_6$ (100 mg, 0.032 mmol, 1 equiv) and toluene (8 mL). A separate 20 mL scintillation vial was loaded with 1,2-di(4-pyridyl)ethylene (bpy_π; 15 mg, 0.080 mmol, 2.5 equiv). The solution of $Co_3(py)_3Co_6Se_8L_6$ was rapidly passed through a plug of Celite on a pipet filter into the vial containing bpy_π. The filter cake was rinsed with toluene (2 mL) and the solution was kept still at 60 °C for 48 h. Within 12 h, a crop of dark red prismatic crystals had deposited along the walls of the vial. After 48 h, the mother liquor was decanted, and crystals were soaked in toluene (5 x 3 mL; 15 minutes each cycle), decanting the supernatant after each treatment. Volatiles were then removed under reduced pressure at 90 °C for 12 h to yield $Co_3(bpy_\pi)_{1.5}Co_6Se_8L_6$ (**2-bpy_π**; 62 mg, 0.020 mmol, 61%) as a dark red crystalline solid. The crystals are insoluble in DCM and toluene, but readily dissolve in d_5-pyridine. ^{1}H NMR analysis reveals in the latter case a clean conversion to $Co_3(py)_3Co_6Se_8L_6$ and the bpy_π linker (Figure S5).

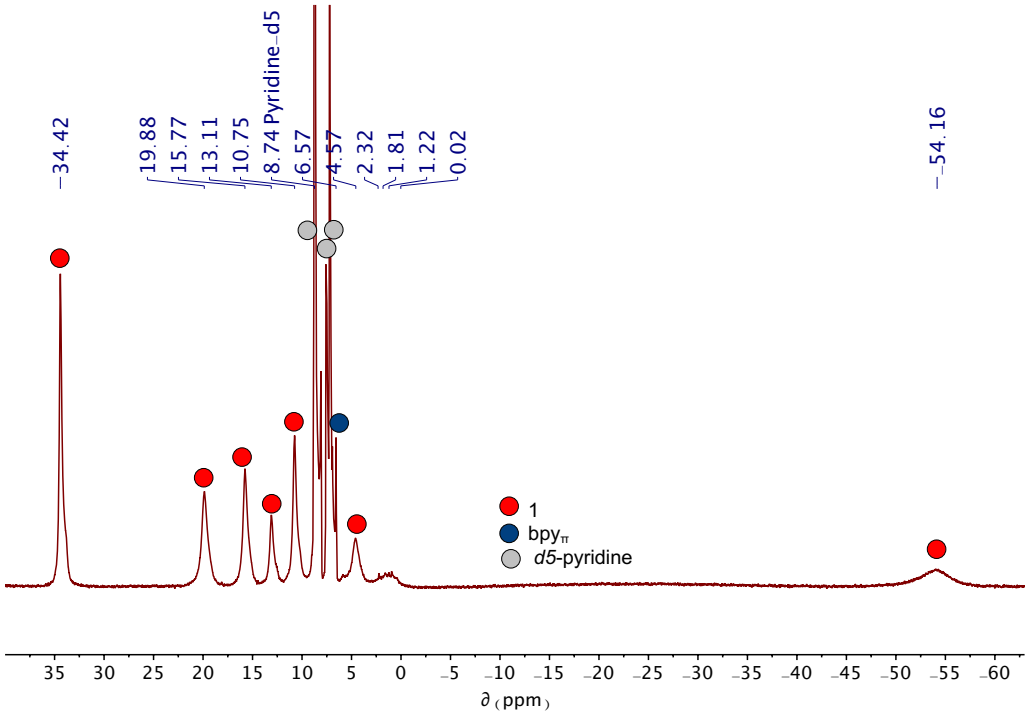

Figure S5. ^{1}H NMR (d_5-pyr, 25 °C, 300 MHz) analysis of **2-bpy$_\pi$** post-dissolution in d_5-pyridine.

S2.4 Synthesis and Isolation of $Co_3(bpy_\sigma)_{1.5}Co_6Se_8L_6$ (2-bpy$_\sigma$)

A 20 mL scintillation vial was loaded with $Co_3(py)_3Co_6Se_8L_6$ (100 mg, 0.032 mmol, 1 equiv) and toluene (8 mL). A separate 20 mL scintillation vial was loaded with 1,2-bi(4-pyridyl)ethane (bpy$_\sigma$; 15 mg, 0.080 mmol, 2.5 equiv). The solution of $Co_3(py)_3Co_6Se_8L_6$ was rapidly passed through a plug of Celite on a pipet filter into the vial containing bpy$_\sigma$. The vial and filter cake were rinsed with toluene (2 mL). The vial was then kept still and heated at 60 °C for 48 h. A layer of dark red prismatic crystals was deposited along the walls of the vial within 12 h. After 48 h, the mother liquor was decanted, and the crystals were soaked in toluene (5 x 3 mL; 15 minutes each cycle), decanting the supernatant between each wash. Volatiles were then removed under reduced pressure at 90 °C for 12 h to yield $Co_3(bpy_\sigma)_{1.5}Co_6Se_8L_6$ (**2-bpy$_\sigma$**; 59 mg, 0.019 mmol, 58%) as a dark red, crystalline solid. The crystals are insoluble in DCM and toluene, although they can be dissolved in coordinating solvents such as d_5-pyridine for ^{1}H NMR analysis, revealing a clean conversion to $Co_3(py)_3Co_6Se_8L_6$ and the bpy$_\sigma$ linker (Figure S6).

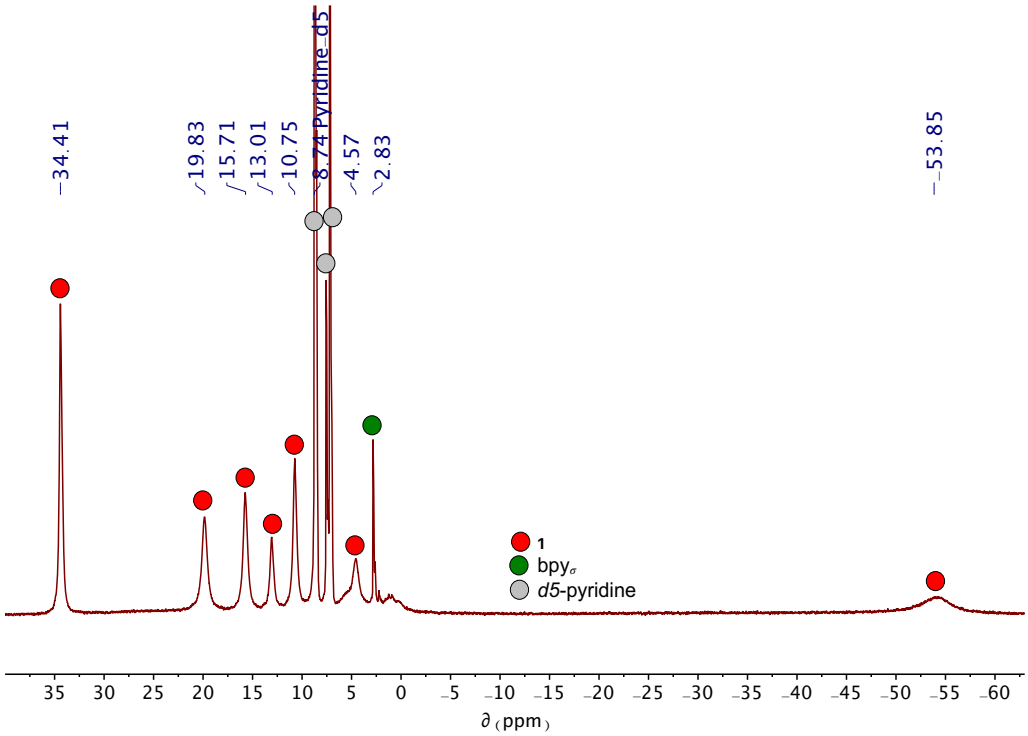

Figure S6. ^{1}H NMR (d_5-pyr, 25 °C, 300 MHz) analysis of **2-bpy$_\sigma$** post-dissolution in d_5-pyridine.

S2.5 Synthesis and Isolation of $[Co_3(bpy_\sigma)_{1.5}Co_6Se_8L_6][TCNE]_2$ ($[2\text{-}bpy_\sigma][TCNE]_2$)

A 20 mL scintillation vial was loaded with **2-bpy$_\sigma$** (41 mg, 0.013 mmol, 1 equiv) and toluene (1 mL). A separate 20 mL scintillation vial was loaded with TCNE (8 mg, 0.065 mmol, 5 equiv), toluene (1 mL) and *n*-pentane (7 mL). The solution of TCNE was passed through a plug of Celite on a pipet filter into the slurry of **2-bpy$_\sigma$**. The filter cake was rinsed with *n*-pentane (1 mL). The mixture was kept still at 25 °C for 24 h. The supernatant was decanted, and the solids were soaked in toluene (3 x 3 mL; 15 minutes each cycle) followed by *n*-pentane (3 x 3 mL; 15 minutes each cycle) before volatiles were removed under reduced pressure to yield $[Co_3(bpy_\sigma)_{1.5}Co_6Se_8L_6][TCNE]_2$ ($[\mathbf{2\text{-}bpy_\sigma}][TCNE]_2$) as a dark red crystalline solid (41 mg, 0.012 mmol, 95%). ATR-FTIR (powder): ν_{CN} = 2182 (s), 2142 (s) cm^{-1}.

$[\mathbf{2\text{-}bpy_\sigma}][TCNE]_2$ can be dissolved in d_5-pyridine, producing bpy$_\sigma$ and, presumably, $[\mathbf{1}][TCNE]_2$ (Figure S8). ^{1}H NMR (d_5-pyr, 300 MHz) δ: 31.96 (s, $\nu_{1/2}$ = 54 Hz); 18.32 (s, $\nu_{1/2}$ = 70 Hz); 15.21 (s, $\nu_{1/2}$ = 51 Hz), 13.03 (s, $\nu_{1/2}$ = 60 Hz); 11.83 (s, $\nu_{1/2}$ = 50 Hz); 5.92 (s, $\nu_{1/2}$ = 84 Hz); –52.11 (s, $\nu_{1/2}$ = 621 Hz) ppm.

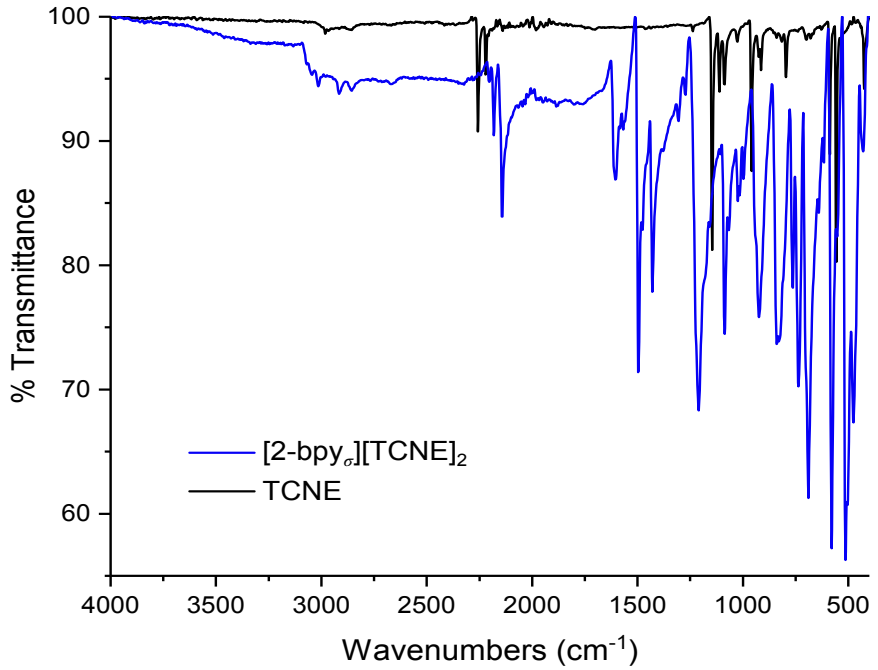

Figure S7. ATR-FTIR spectra of [**2-bpy$_\sigma$**][TCNE]$_2$ (blue) and neutral TCNE (black), displaying the full spectral window acquired (zoom-in on the CN stretches included in Figure 6b).

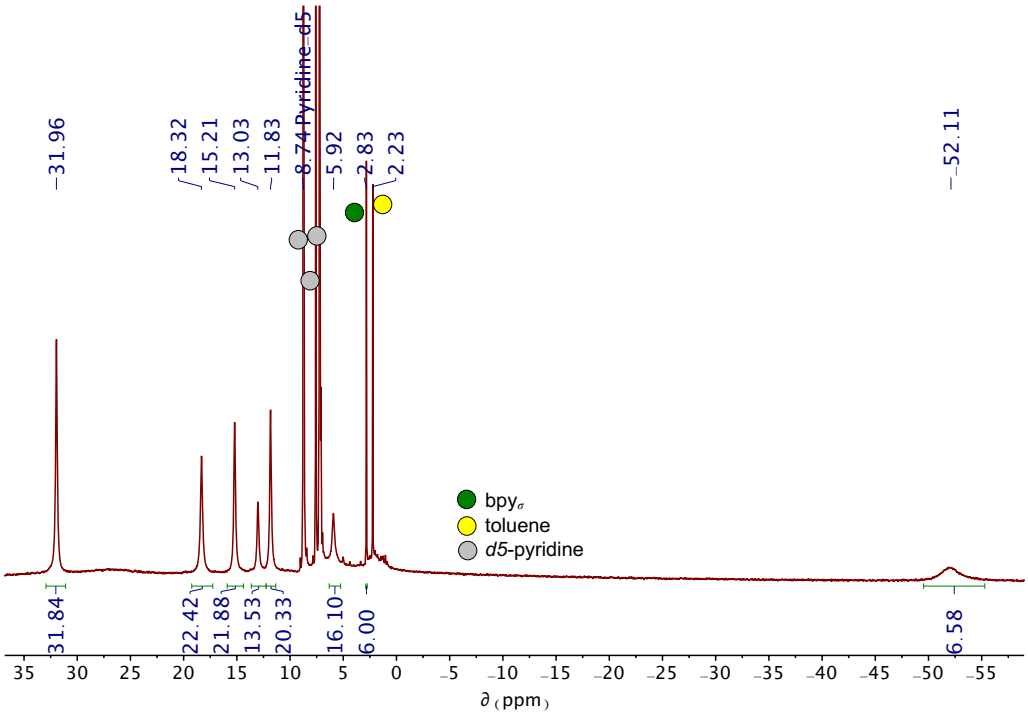

Figure S8. ^{1}H NMR (d_5-pyr, 25 °C, 300 MHz) analysis of [**2-bpy$_\sigma$**][TCNE]$_2$ post-dissolution in d_5-pyridine.

S3 Magnetic Characterization

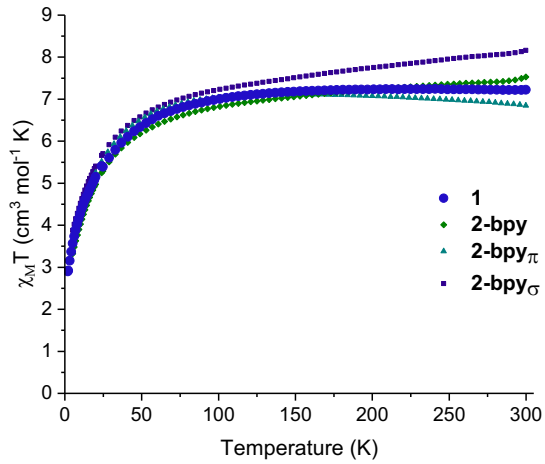

Figure S9. A comparison of the variable-temperature dc magnetic susceptibility of **1**, **2-bpy**, **2-bpy$_\pi$**, and **2-bpy$_\sigma$** recorded at 0.1 T. We attribute the slight deviation in the data recorded for **2-bpy$_\sigma$** to a small amount of an unidentified impurity.

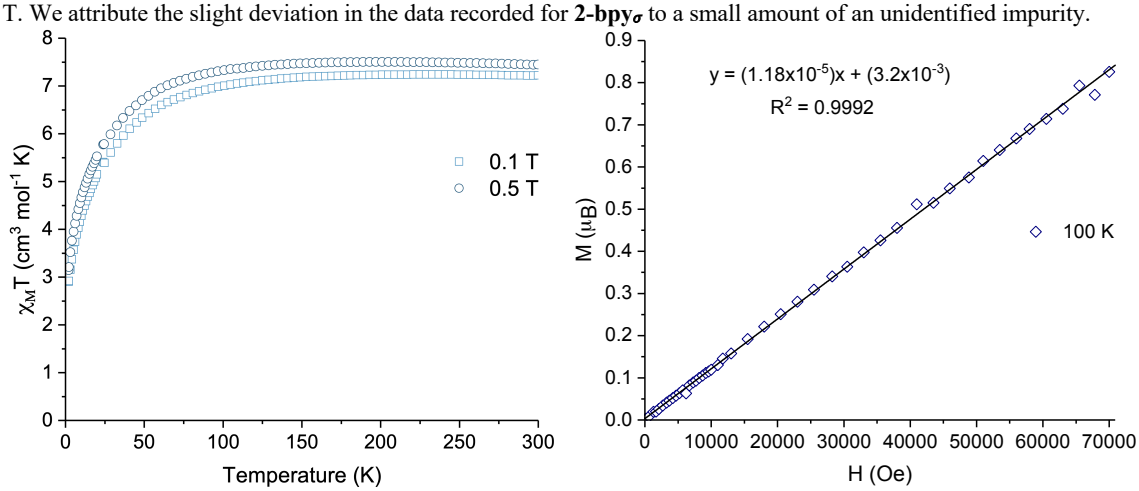

Figure S10. (left) Variable-temperature dc magnetic susceptibility of **1** recorded at 0.1 and 0.5 T, upon warming from 2 to 300 K. (right) Magnetization of **1** recorded between 0 and 7 T at 100 K. These plots indicate that the sample is free of ferromagnetic impurities.

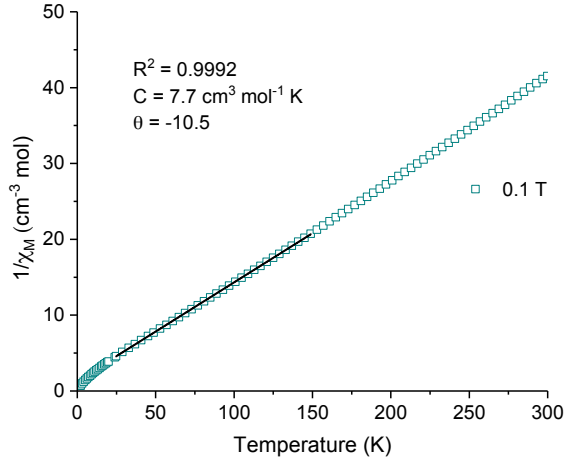

Figure S11. Inverse molar susceptibility of **1** recorded upon warming from 2 to 300 K at 0.1 T. A linear fit to the data between 25 and 150 K, which was used to calculate Curie (C) and Weiss (θ) constants.

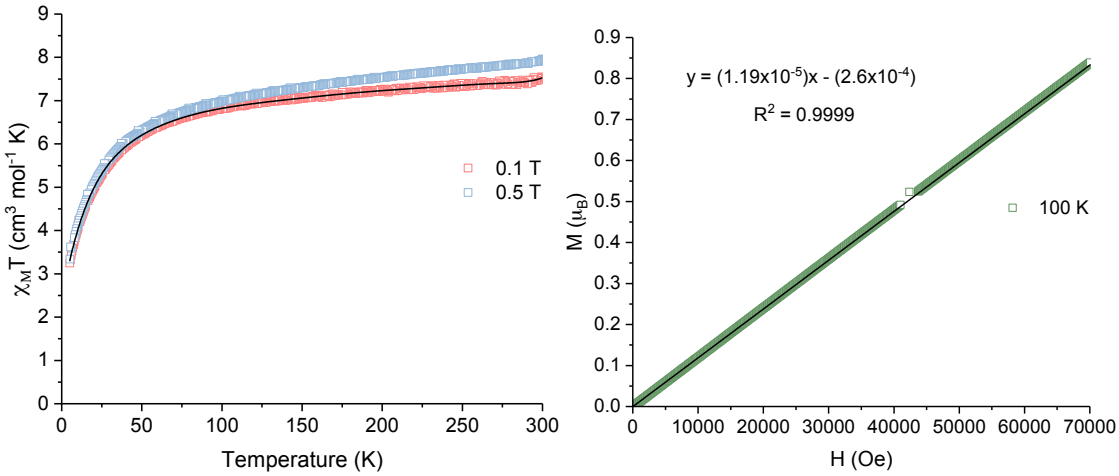

Figure S12. (left) Variable-temperature dc magnetic susceptibility of **2-bpy** recorded at 0.1 and 0.5 T upon warming from 5 to 300 K. The polynomial fit (R^2 = 0.9999) to the data recorded at 0.1 T was used to generate a truncated data set for the susceptibility of **2-bpy** shown Figure S8 above. (right) Magnetization of **2-bpy** recorded at 100 K between 0 and 7 T. These plots indicate the absence of ferromagnetic impurities.

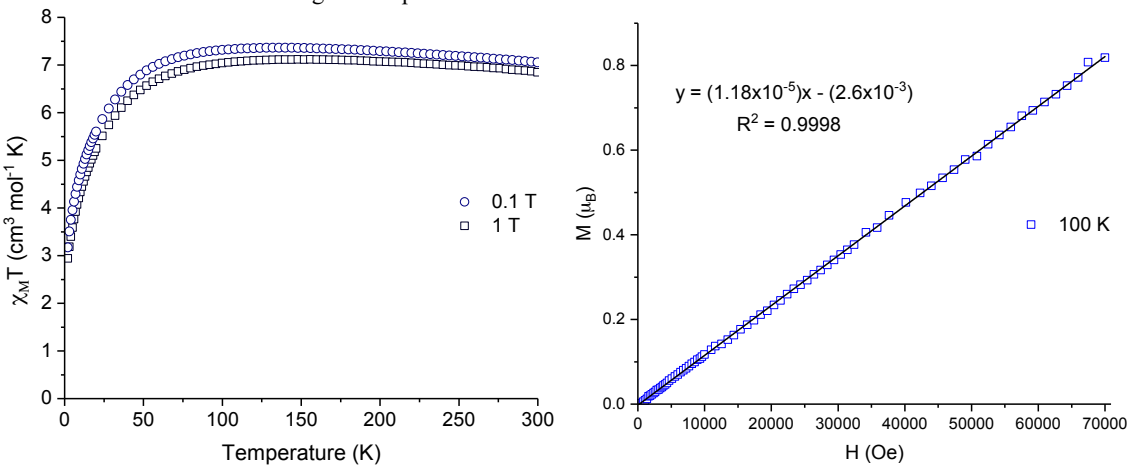

Figure S13. (left) Variable-temperature dc magnetic susceptibility of **2-bpy**$_\pi$ recorded at 0.1 and 1 T upon warming from 2 to 300 K. (right) Magnetization of **2-bpy**$_\pi$ recorded between 0 and 7 T at 100 K. These plots confirm the absence of ferromagnetic impurities.

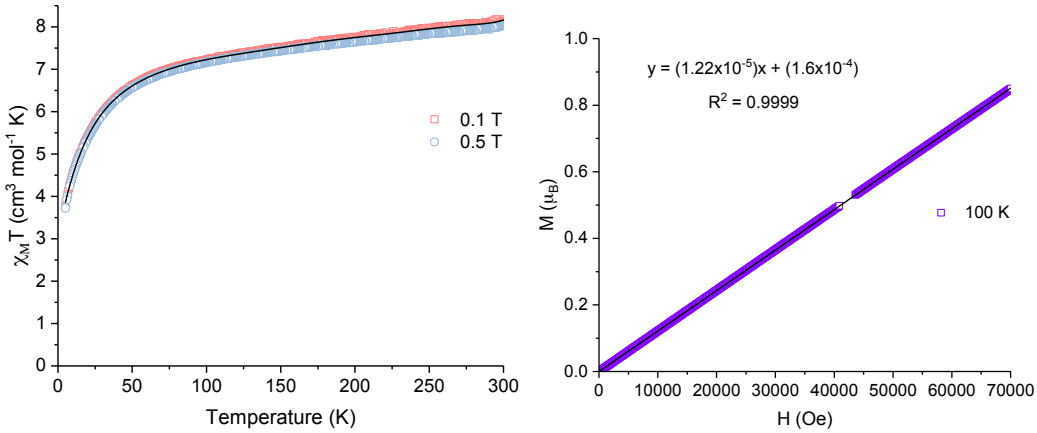

Figure S14. (left) Variable-temperature dc magnetic susceptibility of **2-bpy**$_\sigma$ recorded at 0.1 and 0.5 T, upon warming from 5 to 300 K. The polynomial fit to the data (R^2 = 0.9999) recorded at 0.1 T was used to generate the truncated data set for the susceptibility of **2-bpy**$_\sigma$ shown Figure S8 above. (right) Magnetization of **2-bpy**$_\sigma$ recorded between 0 and 7 T at 100 K. Both plots indicate the absence of ferromagnetic impurities.

S4 Electrochemistry

Large peak-to-peak separation potentials (ΔE_p) indicate that all of these redox processes are quasi-reversible. To gauge the chemical reversibility of these electrochemical transformations, cyclic voltammograms were recorded at several scan rates between 20 and 500 mV s^{-1}. For a chemically reversible process, peak anodic and cathodic currents should exhibit a linear dependence on the square root of the scan rate.[3] This is demonstrated by fitting the electrochemical data to the Randles–Sevcik equation: $j_p = 269000 n_e^{3/2} D_0^{1/2} C_0 v^{1/2}$, where j_p is the current density in A/cm^2, n_e is the number of electron equivalents transferred in the redox process, D_0 is the diffusion coefficient in cm^2/s, C_0 is the bulk concentration in mol/cm^3, and v is the potential scan rate in V/s.

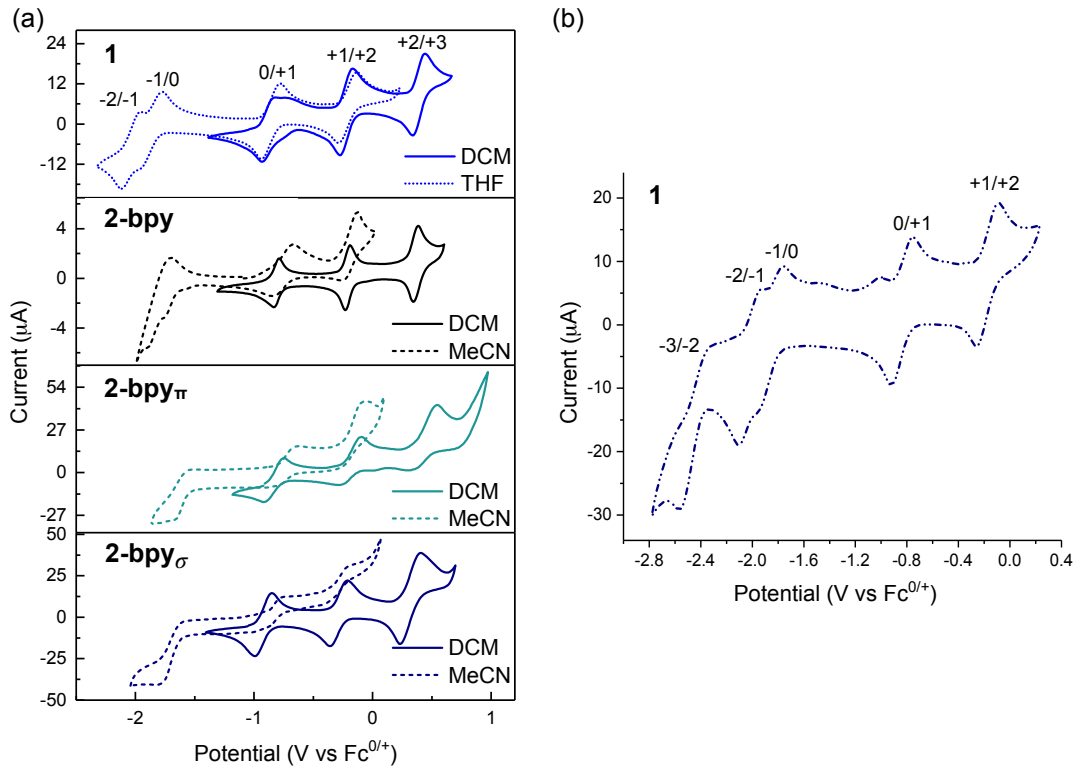

Figure S15. (a) A comparison of the solution-phase cyclic voltammograms recorded for **1** to the solid-state cyclic voltammograms recorded for **2-bpy**, **2-bpy$_\pi$**, and **2-bpy$_\sigma$** in THF, DCM, or MeCN solutions with 0.1 M $TBAPF_6$ electrolyte. The solid-state voltammograms for **2-bpy**, **2-bpy$_\pi$**, and **2-bpy$_\sigma$** were obtained by dropcasting crystalline material on a glassy carbon working electrode. (b) A cyclic voltammogram of **1** in 0.1 M $TBAPF_6$ THF, revealing a third, irreversible reduction event (n_{red}/n_{ox} = –3/–2) at –2.45 V. All voltammograms were recorded with a scan rate of 200 mV/s.

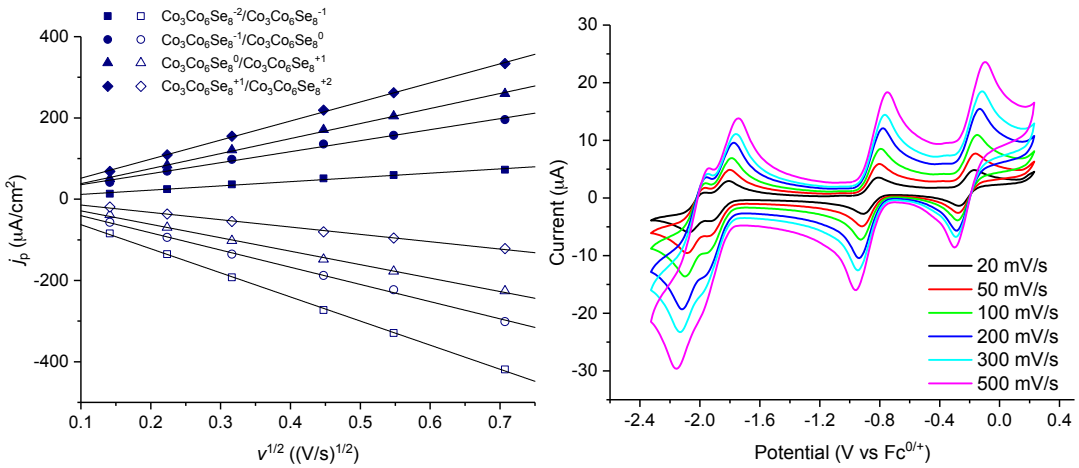

Figure S16. (left) A plot of current density (j_p) versus the square root of scan rate ($v^{1/2}$) for $Co_3(py)_3Co_6Se_8L_6$ in 0.1 M $TBAPF_6$ THF. Linear fits were used to extract diffusion coefficients using the Randles-Sevcik equation. (right) Cyclic voltammograms of $Co_3(py)_3Co_6Se_8L_6$ recorded in 0.1 M $TBAPF_6$ THF.

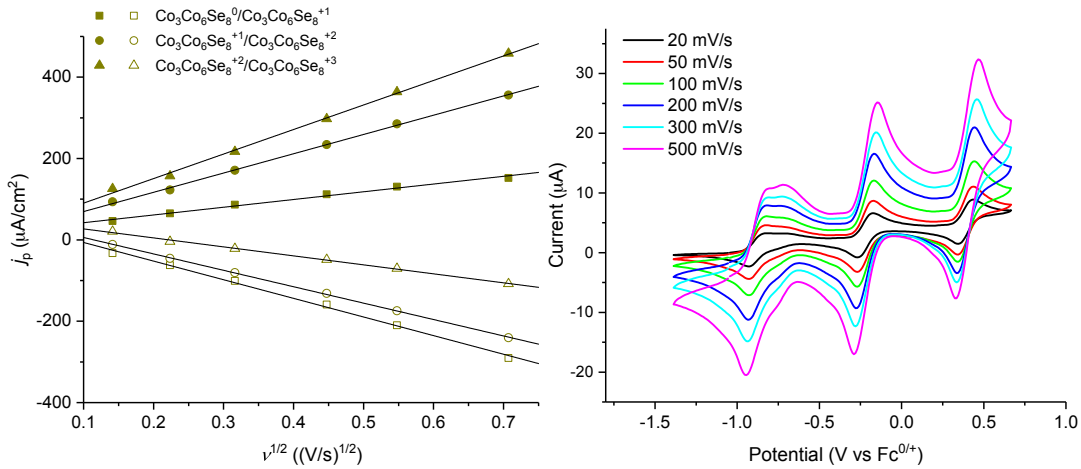

Figure S17. (left) A plot of current density (j_p) versus the square root of scan rate ($v^{1/2}$) for $Co_3(py)_3Co_6Se_8L_6$ in 0.1 M $TBAPF_6$ DCM. Linear fits were used to extract diffusion coefficients using the Randles-Sevcik equation. (right) Cyclic voltammograms of $Co_3(py)_3Co_6Se_8L_6$ recorded in 0.1 M $TBAPF_6$ DCM.

Table S1. Half-wave potentials ($E_{1/2}$), peak-to-peak separation potentials (ΔE_p), and open circuit potentials (OCP) of $Co_3(py)_3Co_6Se_8L_6$ recorded in 0.1 M $TBAPF_6$ DCM or (THF) at 200 mV/s.

redox couple (n_{red}/n_{ox})	$E_{1/2}$ (V vs $Fc^{0/+}$); ΔE_p (mV) $Co_3(py)_3Co_6Se_8L_6$
+2/+3	0.39; 111
+1/+2	–0.22 (–0.21); 111 (162)
0/+1	–0.84 (–0.86); 192 (161)
–1/0	(–1.86); (181)[a]
–1/–2	(–2.03); (163)[a]
OCP (V vs $Fc^{0/+}$)	–1.04 (–0.976)

[a]Due to overlap between the –2/–1 and –1/0 redox couples, these values were approximated based on the location of the shoulders generated by the –2/–1 anodic and –1/0 cathodic currents.

Table S2. Diffusion coefficients (D_0) obtained by applying the Randles–Sevcik equation assuming n_e=1 for various oxidation states determined from cyclic voltammograms of $Co_3(py)_3Co_6Se_8L_6$ recorded in 0.1 M $TBAPF_6$ DCM or (THF).

oxidation state (n)	D_0 (10^{-6} cm^2/s)[a] $Co_3(py)_3Co_6Se_8L_6$
+3	(0.29)[b]
+2	11.1[b] (0.61)
+1	5.10 (2.16)
0	3.02 (3.79)
–1	1.92 (7.91)
–2	0.25

[a] Diffusion coefficients were calculated for each anodic and cathodic peak current density for scan rates ranging between 20 and 500 mV/s, then averaged for all scan rates to obtain the listed values. [b] Calculated using the anodic or cathodic current densities for the (+2/+3) redox couple as measured in 0.1 M $TBAPF_6$ DCM. Values shown with and without parentheses were calculated from cathodic or anodic current densities, respectively.

Table S3. Half-wave potentials ($E_{1/2}$), peak-to-peak separation potentials (ΔE_p), and open circuit potentials (OCP) of **2-bpy**, **2-bpy$_\pi$**, and **2-bpy$_\sigma$** recorded in 0.1 M $TBAPF_6$ DCM or (MeCN) at 200 mV/s.

redox couple (n_{red}/n_{ox})	$E_{1/2}$ (V vs $Fc^{0/+}$); ΔE_p (mV)		
	2-bpy	**2-bpy$_\pi$**	**2-bpy$_\sigma$**
+2/+3	0.36; 41	0.43; 242	0.32; 165
+1/+2	–0.21 (–0.19); 40 (131)	–0.19 (–0.18); 192 (242)	–0.28 (–0.29); 151 (190)
0/+1	–0.81 (–0.76); 50 (171)	–0.83 (–0.74); 171 (243)	–0.92 (–0.86); 143 (211)
–1/0	(–1.74); (71)	(–1.59); (172)	(–1.69); (201)
–1/–2	--	--	--
OCP (V vs $Fc^{0/+}$)	–1.10 (–1.08)	–0.91 (–0.88)	–1.04 (–0.89)

S5 X-ray Diffraction Studies

Single crystals suitable for X-ray analysis were coated in deoxygenated paratone oil and mounted on a 20 µm CryoLoop™ (Hampton Research, 18 mm mount, 0.2 to 0.3 mm loop diameter). Data was collected at –173 °C on a Bruker APEX II single crystal X-ray diffractometer, with a Mo source. Data was integrated and scaled using SAINT, SADABS within the APEX2 software package by Bruker.[5] Solution by direct methods (SHELXT[6] or SIR97[7,8]) produced a complete heavy atom phasing model consistent with the proposed structure. Structures were completed by difference Fourier synthesis with SHELXL.[9–11] Scattering factors are from Waasmair and Kirfel.[12] Hydrogen atoms were placed in geometrically idealized positions and constrained to ride on their parent atoms with C–H distances in the range 0.95–1.00 Å. Isotropic thermal parameters U_{eq} were fixed such that they were $1.2U_{eq}$ of their parent atom Ueq for CHs and $1.5U_{eq}$ of their parent atom U_{eq} in case of methyl groups. All non-hydrogen atoms were refined anisotropically by full-matrix least-squares.

S5.1 $Co_3(py)_3Co_6Se_8L_6$ (1)

Dark-red prismatic crystals of $Co_3(py)_3Co_6Se_8L_6$ (**1**), suitable for single-crystal X-ray diffraction analysis, were grown from a saturated THF solution (3 mL) layered with a mixture of diethyl ether (9 mL) and *n*-pentane (1 mL) over the course of 24 hours at 25 °C. The compound crystallizes in the monoclinic space group $P2_1/c$, and the asymmetric unit contains a singular $Co_3(py)_3Co_6Se_8L_6$ cluster. Each surface Co atom is coordinated by one molecule of pyridine. One of three coordinating pyridine molecules is disordered over two positions. The contribution of the disordered solvent to the diffraction pattern was removed via SQUEEZE.

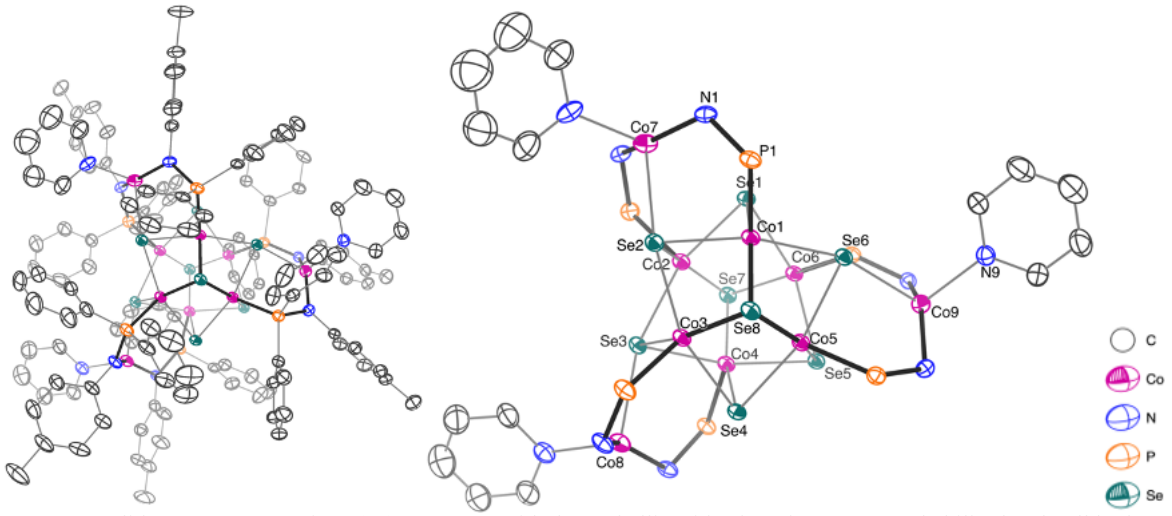

Figure S18. Solid-state structure of $Co_3(py)_3Co_6Se_8L_6$ with thermal ellipsoids plotted at a 50% probability level. All hydrogen atoms are omitted for clarity. Selected interatomic distances (Å): Co(7)-Se(2) 2.534(1), Co(7)-Se(1) 3.200(2), Co(8)-Se(3) 2.524(1), Co(8)-Se(4) 3.243(2), Co(9)-Se(6) 2.573(2), Co(9)-Se(5) 3.147(1), Co(1)-Se(8) 2.334(1), Co(1)-Se(2) 2.347(2), Co(9)-N(9) 2.101(2), Co(7)-N(1) 1.941(2), Se(1)-Se(4) 5.587(2), Se(2)-Se(5) 5.657(3), Se(7)-Se(8) 5.5524(8), Se(3)-Se(6) 5.830(3), Co(1)-Co(2) 2.868(1), Co(3)-Co(4) 2.8383(6), Co(5)-Co(6) 2.831(1), Co(1)-Co(6) 2.8934(6), Co(2)-Co(3) 2.922(1), Co(4)-Co(5) 2.954(1), N(1)-P(1) 1.673(3).

S5.2 $Co_3(bpy)_{1.5}Co_6Se_8L_6$ (2-bpy)

Small dark red, prismatic crystals of $Co_3(bpy)_{1.5}Co_6Se_8L_6$ (**2-bpy**) of sufficient quality for single-crystal X-ray diffractometry were grown from DCM, as described above. The material crystallizes as a 2D, layered reticular solid in the triclinic space group $P\bar{1}$, and the asymmetric unit contains two $Co_9Se_8L_6$ clusters, one (Δ) and one (Λ) enantiomer. The asymmetric unit also contains one full bpy molecule, and four half bpy

molecules. Each bpy molecule is bound to an edge Co(II) site. The contribution of disordered DCM solvent to the diffraction pattern was removed with SQUEEZE. 50 strongly deviating reflections were removed.

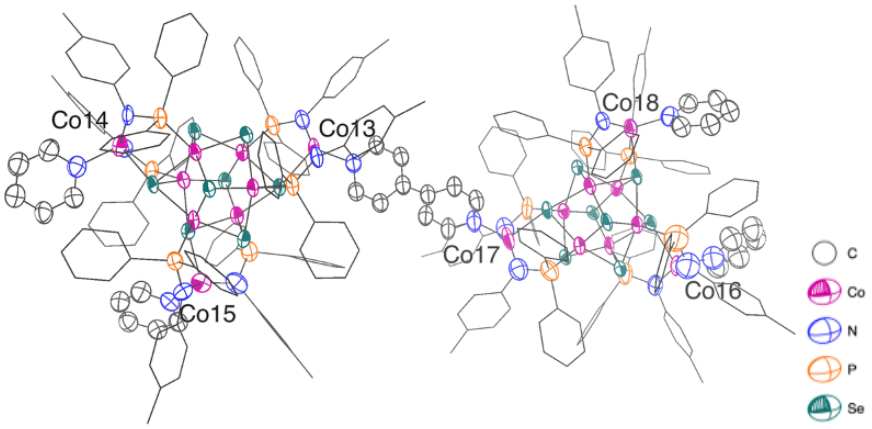

Figure S19. The asymmetric unit of $Co_3(bpy)_{1.5}Co_6Se_8L_6$ (**2-bpy**) with thermal ellipsoids plotted at a 50% probability level. All hydrogen atoms are omitted and phosphinoamide carbon atoms are plotted as wireframes for clarity.

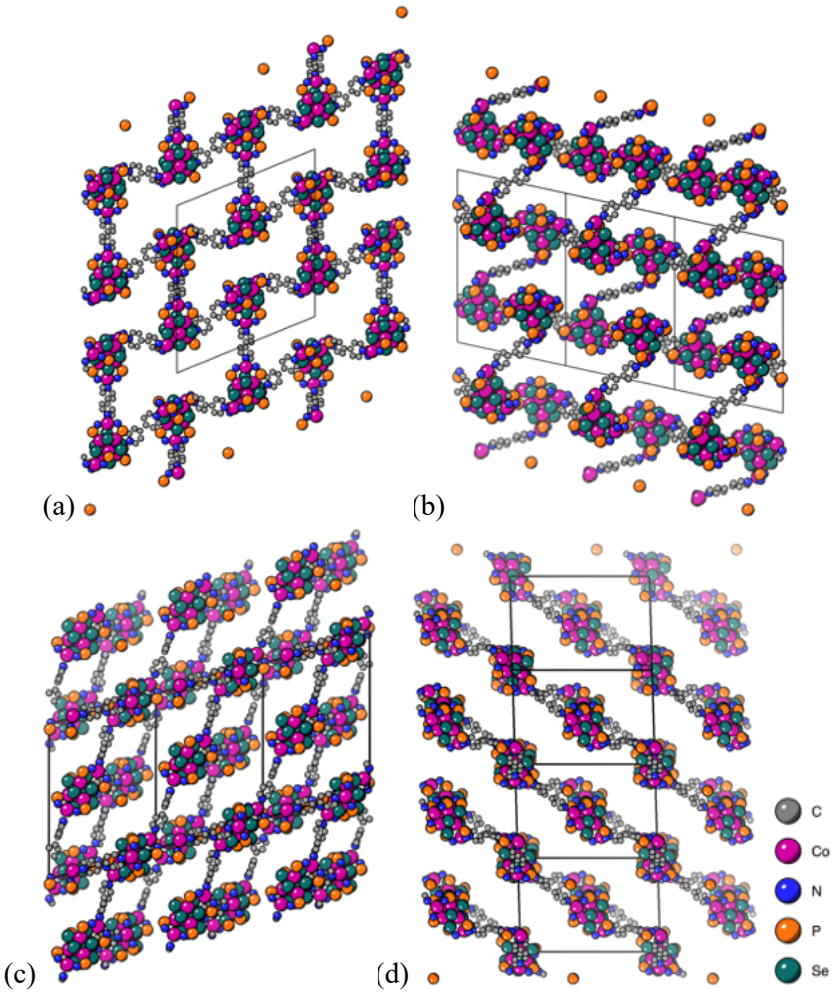

Figure S20. Visualizing the packing of the nanosheets within $Co_3(bpy)_{1.5}Co_6Se_8L_6$ (**2-bpy**). Crystal packing displayed along the (a) [100], (b) [010], (c) [001], (d) [101] lattice planes, illustrating that the 2D sheets are non-coplanar with the lattice indices. Phosphinoamide carbon atoms and all hydrogen atoms are omitted for clarity.

S5.3 $Co_3(bpy_\pi)_{1.5}Co_6Se_8L_6$ (2-bpy_π)

Dark red prismatic crystals of $Co_3(bpy_\pi)_{1.5}Co_6Se_8L_6$ (**2-bpy$_\pi$**) of sufficient quality for single-crystal X-ray analysis were grown from toluene, as described above. The material crystallizes in the triclinic space group $P\bar{1}$. The asymmetric unit contains a single $Co_9Se_8L_6$ cluster with each surface Co(II) site bound by half of a bpy_π molecule. Each cluster is interlinked with three neighboring clusters to produce a 2D layered structure. The contribution of disordered toluene solvent (7 per asymmetric unit) to the diffraction pattern was removed with SQUEEZE.

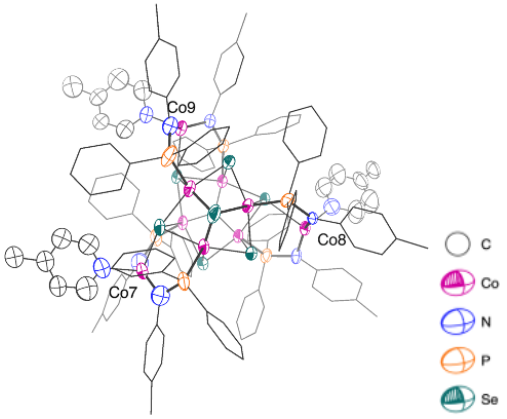

Figure S21. The asymmetric unit of $Co_3(bpy_\pi)_{1.5}Co_6Se_8L_6$ (**2-bpy$_\pi$**) with thermal ellipsoids plotted at a 50% probability level. All hydrogen atoms are omitted and phosphinoamide carbon atoms are plotted as wireframes for clarity.

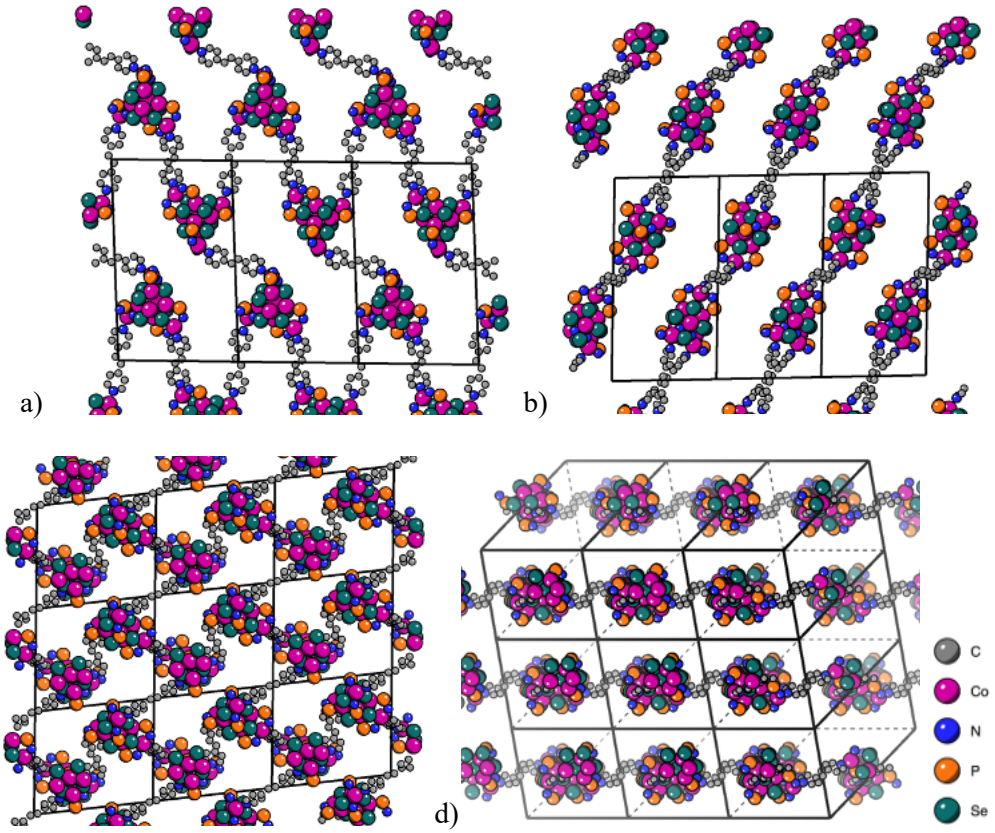

Figure S22. Visualizing the packing of the nanosheets within $Co_3(bpy_\pi)_{1.5}Co_6Se_8L_6$ (**2-bpy$_\pi$**) as viewed along the (a) [100], (b) [010], (c) [001], (d) [111] lattice planes. Phosphinoamide ligand carbon atoms and all hydrogen atoms are omitted for clarity.

S5.4 $Co_3(bpy_\sigma)_{1.5}Co_6Se_8L_6$ (2-bpy$_\sigma$)

Dark red prismatic crystals of $Co_3(bpy_\sigma)_{1.5}Co_6Se_8L_6$ (**2-bpy$_\sigma$**) of sufficient quality for single-crystal X-ray analysis were grown from toluene, as described above. The material crystallizes in the monoclinic space group P 2_1/n. The asymmetric unit contains a single $Co_9Se_8L_6$ cluster with each surface Co(II) site bound by half of a bpy$_\sigma$ molecule. Each cluster is interlinked with three neighboring clusters to produce a 2D layered structure. The contribution of disordered toluene solvent (3 per asymmetric unit) to the diffraction pattern was removed with SQUEEZE. The 50 worst diffraction peaks were eliminated.

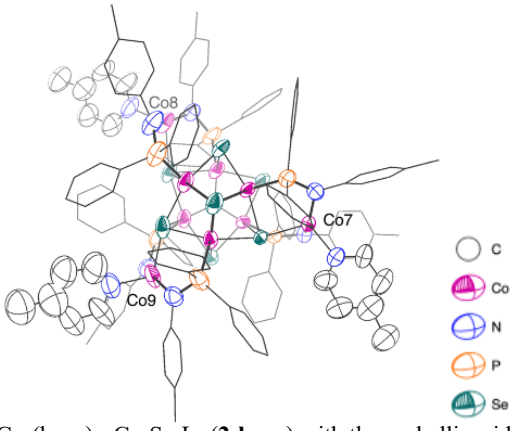

Figure S23. The asymmetric unit of $Co_3(bpy_\sigma)_{1.5}Co_6Se_8L_6$ (**2-bpy$_\sigma$**) with thermal ellipsoids plotted at a 50% probability level. All hydrogen atoms are omitted and phosphinoamide carbon atoms are plotted as wireframes for clarity.

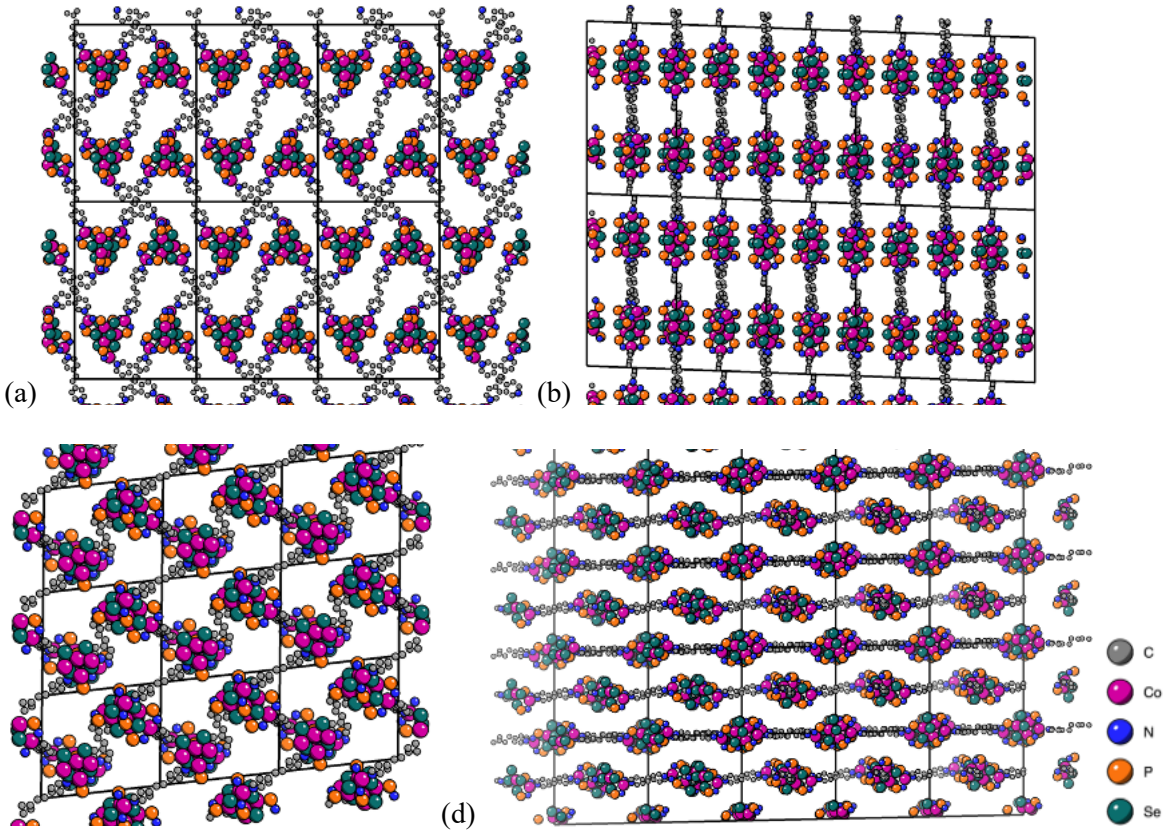

Figure S24. Visualizing the packing of the nanosheets within $Co_3(bpy_\sigma)_{1.5}Co_6Se_8L_6$ (**2-bpy$_\sigma$**) as viewed along the (a) [100], (b) [010], (c) [001], and (d) [011] lattice planes. Phosphinoamide ligand carbon atoms and all hydrogen atoms are omitted for clarity.

S5.5 $[Co_3(bpy_\sigma)_{1.5}Co_6Se_8L_6][TCNE]_2$ ($[\mathbf{2\text{-}bpy_\sigma}][TCNE]_2$)

Dark red crystals of $[Co_3(bpy_\sigma)_{1.5}Co_6Se_8L_6][TCNE]_2$ ($[\mathbf{2\text{-}bpy_\sigma}][TCNE]_2$) of sufficient quality for single-crystal X-ray analysis were produced upon treatment of single-crystalline **2-bpy$_\sigma$** with excess TCNE in a mixture of toluene and *n*-pentane. The intercalated crystals maintain the space group of their precursor **2-bpy$_\sigma$**, monoclinic P 2_1/n. The asymmetric unit contains a single $Co_9Se_8L_6$ cluster with each Co edge site bound by half of a bpy$_\sigma$ molecule, as well as four molecules of toluene and two $[TCNE]^-$ molecules. Each cluster is interlinked with three neighboring clusters to produce a 2D layered structure. A small amount of twinning was observed and accounted for during the refinement. Several 4-tolyl substituents of the aminophosphine ligand framework are disordered, and were modeled over two positions. The contributions of all but one of the intercalated toluene molecules (4 per asymmetric unit) to the diffraction pattern were removed with SQUEEZE. The structure was refined as a two-component twin (twin matrix [1 0 0, 0 –1 0, –0.16 0 –1] with BASF of 0.047). 150 diffraction peaks were still unagreeable.

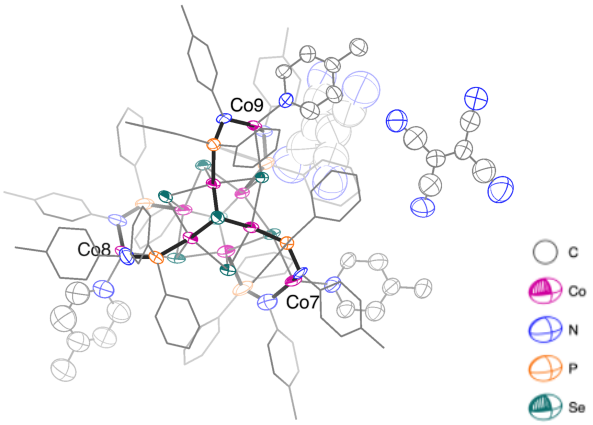

Figure S25. The asymmetric unit of $[Co_3(bpy_\sigma)_{1.5}Co_6Se_8L_6][TCNE]_2$ [**2-bpy$_\sigma$**]$[TCNE]_2$ with thermal ellipsoids plotted at a 50% probability level. All hydrogen atoms are omitted and phosphinoamide carbon atoms are plotted as wireframes for clarity.

S5.6 X-ray Tables

Table S4. Crystallographic data for $Co_3(py)_3Co_6Se_8L_6$ (**1**) and $Co_3(bpy)_{1.5}Co_6Se_8L_6$ (**2-bpy**).

Compound	1	2-bpy
Empirical formula	$C_{129}H_{117}Co_9N_9P_6Se_8$	$C_{258}H_{228}Co_{18}N_{18}P_{12}Se_{16}$
CCDC number	2012111	2012112
Formula weight	3141.18	6276.31
Temperature (K)	100(2)	100(2)
Wavelength (Å)	0.71073	0.71073
Crystal system	Monoclinic	Triclinic
Space group	$P2_1/c$	$P\bar{1}$
a (Å)	30.1353(8)	19.0473(13)
b (Å)	15.1296(5)	28.0304(18)
c (Å)	33.4288(10)	30.824(3)
α (°)	90	109.902(5)
β (°)	116.5790(10)	97.084(5)
γ (°)	90	102.271(4)
Volume (Å^3)	13630.6(7)	14773.8(19)
Z	4	2
ρ^{calc} (g/cm^3)	1.531	1.411
Absorption coefficient (mm^{-1})	3.321	3.064
F(000)	6236	6224
Crystal size (mm^3)	0.150 x 0.140 x 0.090	0.180 x 0.060 x 0.050
Theta range for data collection (°)	1.362 to 28.339	1.353 to 25.545
Index ranges	$-40\leq h\leq 40$, $-20\leq k\leq 20$, $-44\leq l\leq 44$	$-22\leq h\leq 21$, $-33\leq k\leq 34$, $-36\leq l\leq 37$
Reflections collected	66442	87290
Independent reflections	33870 [R(int) = 0.0379]	48703 [R(int) = 0.3504]
Completeness to theta = 25.000°	100.0%	91.1%
Data / restraints / parameters	33870 / 75 / 1474	48703 / 6251 / 2407
Goodness-of-fit on F^2	1.022	1.116
Final R indices [I>2sigma(I)]	R1 = 0.0341, wR2 = 0.0670	R1 = 0.1683, wR2 = 0.3907
R indices (all data)	R1 = 0.0589, wR2 = 0.0729	R1 = 0.4204, wR2 = 0.5253
Largest diff. peak and hole (e$^-$Å^{-3})	1.622 and –0.875	2.629 and –1.813

Table S5. Crystallographic data for $Co_3(bpy_\pi)_{1.5}Co_6Se_8L_6$ (**2-bpy$_\pi$**), $Co_3(bpy_\sigma)_{1.5}Co_6Se_8L_6$ (**2-bpy$_\sigma$**), and $[Co_3(bpy_\sigma)_{1.5}Co_6Se_8L_6][TCNE]_2$ ([**2-bpy$_\sigma$**][TCNE]$_2$).

Compound	**2-bpy$_\pi$ · 7 toluene**	**2-bpy$_\sigma$ · 3 toluene**	**[2-bpy$_\sigma$][TCNE]$_2$ · 4 toluene**
Empirical formula	$C_{181}H_{173}Co_9N_9P_6Se_8$	$C_{153}H_{144}Co_9N_9P_6Se_8$	$C_{172}H_{152}Co_9N_{17}P_6Se_8$
CCDC number	2012109	2012110	2012108
Formula weight	3822.45	3456.91	3804.97
Temperature (K)	100(2)	100(2)	100(2)
Wavelength (Å)	0.71073	0.71073	0.71073
Crystal system	Triclinic	Monoclinic	Monoclinic
Space group	$P\bar{1}$	$P\ 2_1/n$	$P\ 2_1/n$
a (Å)	15.3355(14)	18.3156(16)	19.2673(10)
b (Å)	17.8362(17)	24.1602(18)	23.5145(10)
c (Å)	29.564(3)	35.255(3)	35.6971(18)
α (°)	87.013(6)	90	90
β (°)	87.701(5)	92.120(4)	92.434(3)
γ (°)	82.900(5)	90	90
Volume (Å^3)	8008.9(13)	15590(2)	16158.4(14)
Z	2	4	4
ρ^{calc} (g/cm^3)	1.318	1.355	1.564
Absorption coefficient (mm^{-1})	2.827	2.904	2.818
F(000)	3154	6320	7632
Crystal size (mm^3)	0.130 x 0.080 x 0.060	0.150 x 0.120 x 0.030	0.150 x 0.080 x 0.070
Theta range for data collection (°)	1.314 to 25.091	1.396 to 24.995	1.367 to 25.027
Index ranges	$-14\leq h\leq 14$, $-17\leq k\leq 17$, $-28\leq l\leq 28$	$-21\leq h\leq 21$, $-28\leq k\leq 28$, $0\leq l\leq 41$	$-22\leq h\leq 22$, $-27\leq k\leq 27$, $-42\leq l\leq 42$
Reflections collected	28506	53839	56717
Independent reflections	28506 [R(int) = 0.2693]	27385 [R(int) = 0.1850]	28523 [R(int) = 0.1691]
Completeness to theta = 25.000°	100.0%	99.8%	99.9%
Data / restraints / parameters	28506 / 1772 / 1274	27385 / 2752 / 1308	28523 / 1577 / 1546
Goodness-of-fit on F^2	0.803	1.042	1.087
Final R indices [I>2sigma(I)]	R1 = 0.0856, wR2 = 0.1839	R1 = 0.1364, wR2 = 0.3424	R1 = 0.1854, wR2 = 0.3438
R indices (all data)	R1 = 0.2913, wR2 = 0.2380	R1 = 0.2844, wR2 = 0.3990	R1 = 0.3094, wR2 = 0.3969
Largest diff. peak and hole (e$^-$Å^{-3})	0.817 and –0.649	1.276 and –1.481	2.381 and –1.674

References

(1) Passarelli, V.; Benetollo, F. Reactivity of Novel N,N'-Diphosphino-Silanediamine-Based Rhodium(I) Derivatives. *Inorg Chem* **2011**, *50*, 9958–9967.

(2) Kephart, J. A.; Mitchell, B. S.; Chirila, A.; Anderton, K. J.; Rogers, D.; Kaminsky, W.; Velian, A. Atomically Defined Nano-Propeller Fe3Co6Se8(Ph2PNTol)6: Functional Model for the Electronic Metal-Support Interaction Effect, and High Catalytic Activity for Carbodiimide Formation. *J. Am. Chem. Soc.* **2019**, *141* (50), 19605–19610.

(3) Bain, G. A.; Berry, J. F. Diamagnetic Corrections and Pascal's Constants. *J. Chem. Educ.* **2008**, *85* (4), 532.

(4) Chilton, N. F.; Anderson, R. P.; Turner, L. D.; Soncini, A.; Murray, K. S. PHI: A Powerful New Program for the Analysis of Anisotropic Monomeric and Exchange-Coupled Polynuclear *d* - and *f* - Block Complexes. *J. Comput. Chem.* **2013**, *34* (13), 1164–1175.

(5) *Bruker APEX2 (Version 2.1-4), SAINT (Version 7.34A), SADABS (Version 2007/4*), *2007 BrukerAXS Inc, Madison, Wisconsin, USA.*

(6) Sheldrick, G.M. *Acta Cryst.* **2015**, *A71*, 3-8.

(7) Altomare, A.; Burla, C.; Camalli, M.; Cascarano, G. L.; Giacovazzo, C.; Guagliardi, A.; Moliterni, A.G.G.; Polidori, G.; Spagna, R. *J. Appl. Crystallogr*., **1999**, *32*, 115-119.

(8) Altomare, A.; Cascarano, G. L.; Giacovazzo, C.; Guagliardi, A. *J. Appl. Crystallogr.*, **1993***, 26*, 343-350.

(9) Sheldrick, G. M. *SHELXL-97, Program for the Refinement of Crystal Structures*, **1997**, University of Göttingen, Germany.

(10) Sheldrick, G. M. *Acta Cryst.* **2015***, C71,* 3–8.

(11) Mackay, S.; Edwards, C.; Henderson, A.; Gilmore, C.; Stewart, N.; Shankland, K.; Donald, A. *MaXus: A Computer Program for the Solution and Refinement of Crystal Structures from Diffraction Data*, **1997**, University of Glasgow, Scotland.

(12) Waasmaier, D.; Kirfel, A. *Acta Cryst*., **1995**, *51*, 416-430.